Effect of the deposition technique on the metallurgy and hydrogen storage characteristics of metastable MgyTi(1-y) thin films

Electrochemical and Solid-State Letters, **9** (11) A520-A523 (2006)
1099-0062/2006/9(11)/A520/4/$20.00 © The Electrochemical Society

Effect of the Deposition Technique on the Metallurgy and Hydrogen Storage Characteristics of Metastable $Mg_yTi_{(1-y)}$ Thin Films

P. Vermeulen,[a,z] R. A. H. Niessen,[b] D. M. Borsa,[c] B. Dam,[c] R. Griessen,[c] and P. H. L. Notten[a,b,*]

[a]*Eindhoven University of Technology, 5600 MB Eindhoven, The Netherlands*
[b]*Philips Research Laboratories, 5656 AE Eindhoven, The Netherlands*
[c]*Vrije Universiteit, 1081 HV Amsterdam, The Netherlands*

$Mg_yTi_{(1-y)}$ alloys with $0.50 \leqslant y \leqslant 1.00$ were prepared by electron beam deposition and magnetron co-sputter deposition. The effects of the deposition technique are discussed in two ways; the metallurgy of the as-deposited films and the hydrogen storage characteristics. In spite of the fact that for both preparation methods similar unit cell dimensions are found, the broader X-ray diffraction peaks of e-beam deposited alloys indicate a relatively small grain size. Electrochemical characterization of the compounds upon (de)hydrogenation shows that the deposition method does not significantly influence the hydrogen capacity and kinetics. Moreover, essentially the same cycle-life behavior is found for both types of alloys.
 [DOI: 10.1149/1.2345548]

Manuscript submitted July 6, 2006; revised manuscript received July 24, 2006. Available electronically August 31, 2006.

The development of solid-state materials capable of storing hydrogen with a high volumetric and gravimetric energy density is required for the use of hydrogen as energy carrier in a future hydrogen economy. Solid-state hydrogen storage materials, with a gravimetric storage capacity of 1.1 wt % of hydrogen are already being used on a large scale as metal hydride (MH) electrode in rechargeable nickel-metal hydride (NiMH) batteries.[1,2] Much research effort is still aimed at improving properties of this electrode material, such as corrosion resistance, rate-capability, and reversible hydrogen storage capacity.[3-5] A storage capacity of at least 6 wt % of hydrogen was set by the U.S. Department of Energy to accomplish essential breakthroughs in the field of gas-phase and electrochemically-driven devices.[6] As the commercially available MH materials mentioned above do not satisfy this requirement, new materials must be found. These are often based on Mg, as it is lightweight, cheap, and can reversibly store up to two hydrogen atoms per Mg atom. From a gravimetric point of view, it would be advantageous to use pure Mg as hydrogen storage material. However, several disadvantages related to the extremely poor hydrogen diffusion in the hydrided form prevent pure Mg from being employed.[7]

Several methods have been proposed to circumvent this problem. Wagemans et al. showed that the hydrogen storage properties of Mg can be enhanced by decreasing the particle size of the crystallites.[8] They calculated that decreasing the grain size of magnesium hydride below ~1.3 nm results in a substantial decrease of the hydrogen desorption enthalpy. Another method to enhance the hydrogen storage properties of Mg is to substitute part of the atoms by another element, preferably also lightweight to retain its high energy density. It is well known that alloying magnesium with a transition metal (TM) can result in a significant enhancement of the kinetics, like for example Mg_2Ni. Unfortunately, TMs such as Ti, V, and Cr are immiscible with Mg and alloys can therefore not be prepared by conventional methods.[9] However, Mg was successfully alloyed with Ti, V, and Cr using a complex anvil-cell technique that requires extreme temperatures and pressures.[10-12]

Quite surprisingly, it was recently found that similar Mg-alloys could also be prepared by electron beam deposition at room temperature.[13-15] These alloys were found to be crystalline and single-phase. Electrochemical (de)hydrogenation showed that their hydrogen storage characteristics were enhanced with respect to MgH_2. The reasoning behind this was that the crystal structure of the alloying metal (Sc, Ti, V, and Cr) could be stabilized even up to very high Mg-contents, resulting in more favorable hydrogen transport properties.[16] The experiments indicated that for hydrogen storage purposes the Mg-Ti alloy revealed superior characteristics. Recently, Borsa et al. found that the remarkable optical properties of $Mg_yTi_{(1-y)}H_x$ offer also possibilities for the application of these alloys as switchable smart coating in solar collectors.[17]

In this paper, we show that the relevant properties of MgTi alloys do not depend significantly on the deposition technique by comparing sputtered and e-beam deposited (EBD) films.

Experimental

Electron beam deposited, 200 nm thick, $Mg_yTi_{(1-y)}$ thin films with $0.05 \leqslant y \leqslant 1.00$ were prepared on thoroughly cleaned quartz substrates ($\varnothing$ 20 mm) at low base pressures (1×10^{-8} to 1×10^{-7} mbar). The $Mg_yTi_{(1-y)}$ alloys were coated with 10 nm Pd to prevent oxidation. Moreover, Pd catalyzes the charge transfer reaction during electrochemical (de)hydrogenation. Direct current (dc)/radio frequency (rf) magnetron co-sputtered $Mg_yTi_{(1-y)}$ (y = 0.70, 0.80, and 0.90) thin films with a nominal thickness of 200 nm were prepared on similar substrates. Similar to the EBD films, the $Mg_yTi_{(1-y)}$ layers were covered with 10 nm Pd. Rutherford backscattering spectroscopy (RBS) was used to determine the thickness and composition of the as-deposited thin films which are used to calculate the hydrogen storage capacity. Here, the influence of the Pd layer was not taken into account as the maximum deviation that can occur was limited to 3%. X-ray diffraction (XRD) measurements were performed using a Panalytical X'Pert MPD PRO diffractometer, equipped with a Cu source and a X'Celerator detector. Electrochemical characterization of the metallic films at room temperature in a strong alkaline environment (6 M KOH) was carried out using an Autolab PGSTAT30 (Ecochemie, The Netherlands). Special care was taken to avoid oxygen in the electrolyte as it is known that it can affect, among other things, the electrochemical potential and hydrogen storage capacity.[18] The electrochemical potential was measured vs a Hg/HgO reference electrode (Koslow Scientific Company, USA).[19] The cutoff potential was set to 0 V in all electrochemical experiments.

Results and Discussion

The crystallographic orientation of the thin films prepared by magnetron co-sputtering and EBD was determined by means of XRD. The XRD spectrum of a sputtered $Mg_{0.80}Ti_{0.20}$ thin film is depicted in Fig. 1. A very intense peak was observed at $2\theta = 35.4°$ and is associated with a hexagonal close-packed (hcp) Mg-Ti unit cell. The 002 reflection shifted with respect to the posi-

* Electrochemical Society Active Member.
z E-mail: P.Vermeulen@tue.nl

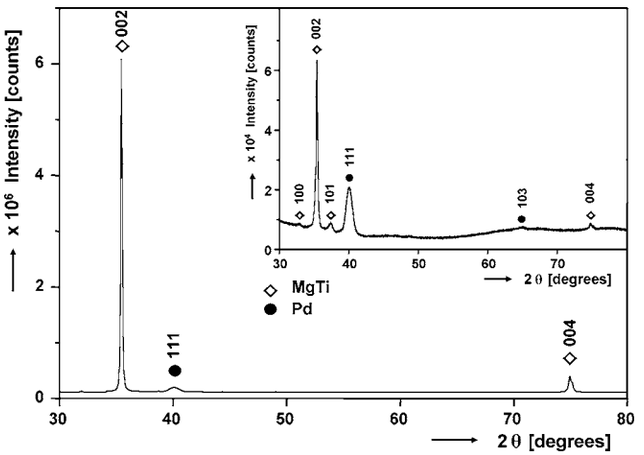

Figure 1. XRD spectrum of an as-deposited $Mg_{0.80}Ti_{0.20}$ thin film with a thickness of 200 nm and a 10 nm thick Pd topcoat prepared by means of dc/rf magnetron co-sputtering. Inset: the XRD spectrum of a similar composition prepared by means of electron beam deposition. Note the difference of the vertical intensity scales.

tions of both pure Mg (34.4° 2θ) and Ti (38.4°2θ) due to a solid solution of Ti in Mg. The shift of the position of the 002 peak to larger angles (smaller interatomic distances) with respect to pure Mg is a direct consequence of the smaller molar volume of Ti as compared to Mg.[20] In contrast to these findings, Richardson et al. and Farangis et al. determined that Mg-Ti thin films, within a similar composition range and also prepared by magnetron co-sputtering, were amorphous.[21,22] Apparently, the deposition conditions (temperature, deposition rate, etc.) influence the crystallography of the films significantly. As a comparison, the XRD spectrum of a $Mg_{0.80}Ti_{0.20}$ alloy prepared by EBD is depicted in the inset in Fig. 1.[15] It is apparent that the intensity of the peaks is different for the two deposition methods. The 002 refection is very intense for the co-sputtered compounds, whereas the EBD thin films show a much weaker reflection. This is discussed in more detail below.

The 002 peaks for EBD and magnetron co-sputtered $Mg_yTi_{(1-y)}$ alloys are shown in Fig. 2. Note that the peaks of the EBD $Mg_{0.50}Ti_{0.50}$ and $Mg_{0.70}Ti_{0.30}$ alloys are not included in this figure as their intensities were extremely low. Due to the intensity difference of the 002 reflections for both deposition techniques, the scale of the *y*-axis is adjusted to depict the peaks appropriately. The most notable observation is that the peak positions seem to be almost independent of the deposition method used, which implies that the geometries of the unit cells of the alloys are very similar. However, the width of the peaks is clearly dependent on the deposition technique. Electron beam deposited $Mg_yTi_{(1-y)}$ layers reveal relatively broad peaks in comparison to sputtered films, indicating a difference in grain size. To quantify the difference, we used the Scherrer equation

$$D = K\lambda/B_{1/2}\cos\theta \quad [1]$$

where D is the diameter of the particle, K is the shape factor (typical value is 0.9), λ is the wavelength of the incident beam (1.54 Å), $B_{1/2}$ is the linewidth in radians at half-maximum peak intensity, and θ is the Bragg angle.[23] $B_{1/2}$ must be corrected for broadening originating from the instrument (B_{instr}) and takes the form

$$B^2_{1/2} = B^2_{obs} - B^2_{instr} \quad [2]$$

where B_{obs} is the observed width. However, as in our case

$$B_{obs} \gg B_{instr} \quad [3]$$

Eq. 1 simplifies to

$$D = K\lambda/B_{obs}\cos\theta \quad [4]$$

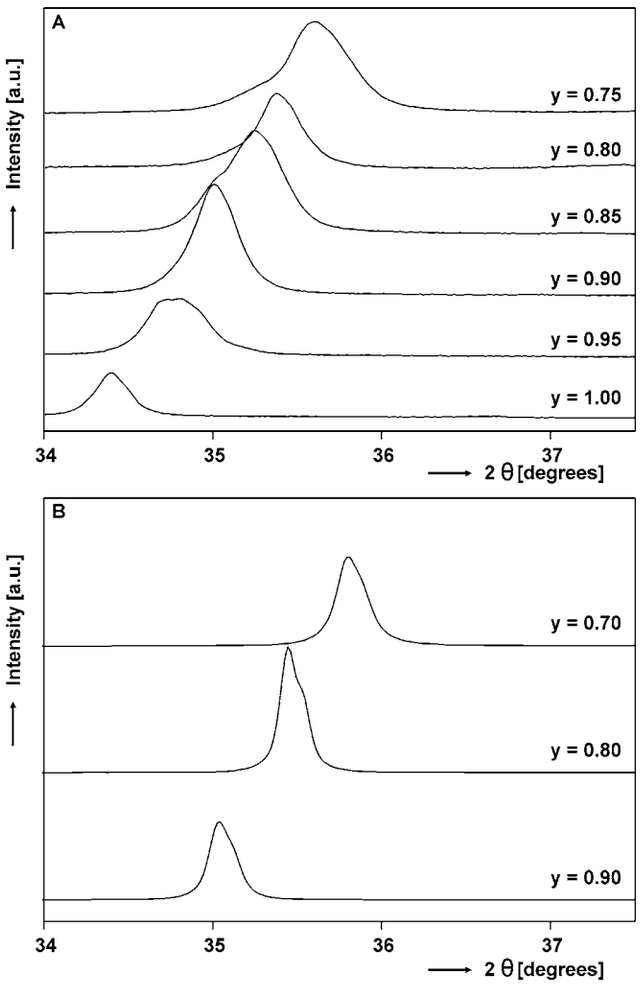

Figure 2. Evolution of the 002 reflection as a function of Ti-content for (A) e-beam deposited and (B) magnetron co-sputtered $Mg_yTi_{(1-y)}$ alloys.

Before determining the grain size it must be noted that the 002 peaks of the films have a double-peak structure, which is most pronounced for the sputtered films due to their relatively narrow peaks. This structure is caused by the fact that Cu radiation used in the XRD measurements consists of two characteristic lines, viz. Cu $K\alpha_1$ (λ = 1.5404 Å) and Cu $K\alpha_2$ (λ = 1.5443 Å). Keeping in mind that the linewidth at half-maximum peak intensity ($B_{1/2}$) is related to one of the peaks, we obtain, on average, a particle diameter of 28 nm for EBD compounds and 52 nm for sputtered alloys. This difference must be due to the deposition technique and the associated deposition conditions as the chemistry is the same.

To determine the effects of the deposition technique on the hydrogen storage properties, electrochemical measurements are performed to (de)hydrogenate the metallic films. In general, two reactions are involved in (de)hydrogenation. Starting from the as-deposited state, H_2O is reduced at the metal (M) surface to form adsorbed hydrogen atoms (H_{ad}) and hydroxyl ions. This reaction can be represented by

$$M + H_2O + e^- \Leftrightarrow MH_{ad} + OH^- \quad [5]$$

Hereafter, H_{ad} is absorbed into the crystal lattice of the host metal and forms absorbed atomic hydrogen (H_{abs}) according to

$$MH_{ad} \Leftrightarrow MH_{abs} \quad [6]$$

During dehydrogenation the reverse reactions take place.

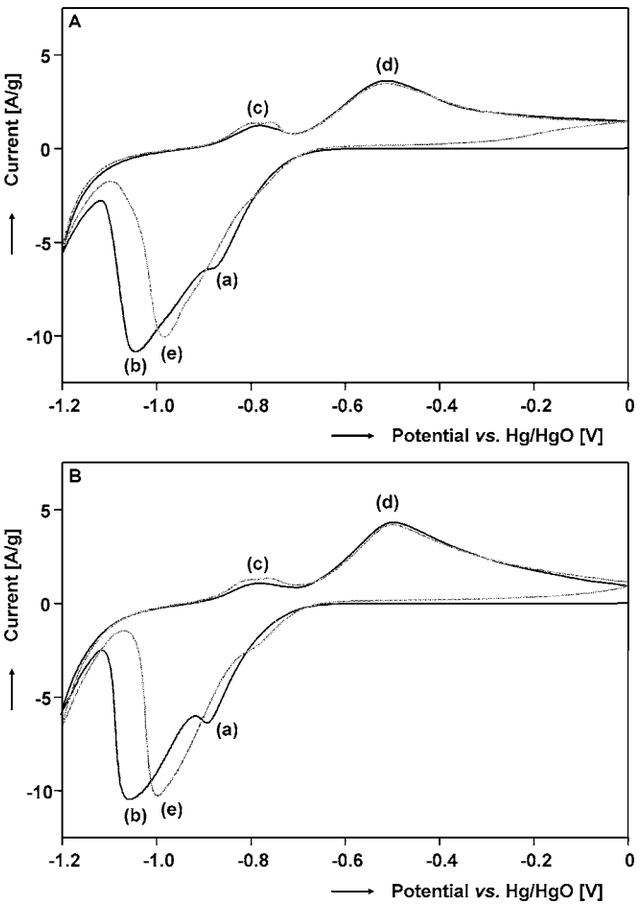

Figure 3. CVs of (A) e-beam deposited and (B) magnetron co-sputtered $Mg_{70}Ti_{30}$ films in the range 0 to − 1.2 V using a scan rate of 0.5 mV/s. The specific features of the curves are denoted (a) to (e).

Figure 3 shows the cyclic voltammograms (CVs) of the first two cycles of $Mg_{0.70}Ti_{0.30}$ films in the range −1.2 to 0 V using a scan rate of 0.5 mV/s. This particular range is chosen because previous galvanostatic measurements showed that within this range the (de)hydrogenation reactions of MgTi alloys take place.[14,15] Starting from the as-deposited state of the e-beam deposited alloy at 0 V (Fig. 3A, black curve), there is nearly no current flowing down to a potential of −0.7 V. Hereafter, the current decreases toward more negative values and reaches a local minimum at −0.88 V denoted by (a). This peak, which is also observed during galvanostatic measurements, has been attributed to the irreversible hydrogenation part of the compound.[14,15] Decreasing the potential beyond −0.88 V results in a small plateau, however, it quickly declines again down to −11 A/g at −1.04 V (peak b). The corresponding reaction is further hydrogenation of the $Mg_{0.70}Ti_{0.30}$ alloy and a phase transition is most likely involved. After the maximum H storage capacity is reached, the current increases, only to decrease rapidly at more negative potentials due to the formation of hydrogen gas according to

$$2MH_{ad} \Leftrightarrow 2M + H_2(1) \qquad [7]$$

During scanning toward less negative potentials, the first peak (c) observed is related to a broad β-solid solution, commonly found for $Mg_yTi_{(1-y)}$ alloys.[14,15] Also, a small peak is observed and can be related to the dehydrogenation of the Pd topcoat. Hereafter, the $Mg_{0.70}Ti_{0.30}H_x$ transforms from β to the α phase which manifests itself at −0.51 V (peak d). During the second hydrogenation (gray curve), the first cathodic peak (e) corresponds to hydrogenating the

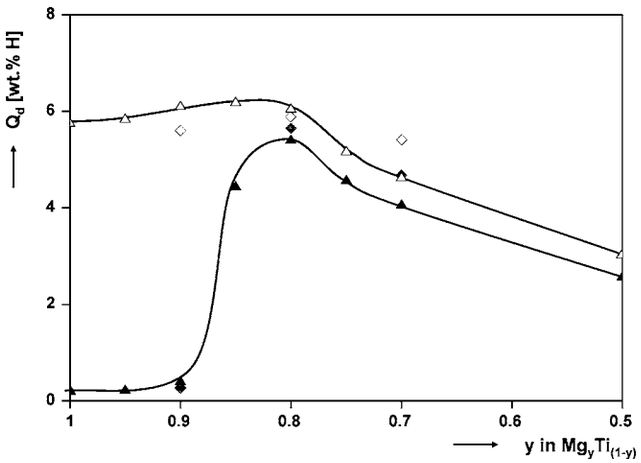

Figure 4. Discharge capacity (Q_d) vs the Mg-content in $Mg_yTi_{(1-y)}$ alloys. A distinction is made between the discharge capacity obtained using high-rate discharging (+0.12 mA; closed symbols) and low-rate discharging (+0.012 mA; open symbols). The data corresponding to electron beam deposited thin films are represented by triangles, whereas magnetron co-sputtered compounds are indicated by diamonds.

MgTi alloy. Note that in line with the comments above, the second hydrogenation does not show any features that resemble peak (a) in the first hydrogenation, illustrating its irreversible nature. The irreversibility of the hydrogenation leads to a lower hydrogenation capacity during the second hydrogen insertion. Moreover, it is evident that the overpotential necessary for the second hydrogenation reaction to proceed steadily is significantly decreased in comparison to the first cycle. In contrast, the peak positions and peak areas during the first and second dehydrogenation are not significantly changed illustrating that the rate-capability as well as the reversible H storage capacity are approximately constant. Figure 3B shows that very similar voltammograms are observed for the magnetron co-sputtered $Mg_{0.70}Ti_{0.30}$ thin film, stressing that the electrochemistry of both layers is approximately analogous.

The effect of the Ti-content in $Mg_yTi_{(1-y)}$ alloys on the discharge capacity (Q_d) is determined by first hydrogenating the metallic layers with a current of −0.6 mA. Hereafter, a high-rate current (+0.12 mA) and additionally a low-rate current (+0.012 mA) are used to extract the hydrogen atoms. The corresponding H discharge capacities are shown for e-beam deposited and sputtered films in Fig. 4. For both preparation methods, the $Mg_{0.80}Ti_{0.20}$ composition exhibits the highest reversible hydrogen storage capacity of ~6 wt % of H. Moreover, its reversible H capacity using high-rate discharging, i.e., within 2 h at room temperature, is superior to the other compositions, indicating a good rate-capability. This is especially desirable for high-drain applications where the need of a high current is vital for the device to work properly. In Fig. 4 the dependence of the composition reveals two specific regions; for $Mg_yTi_{(1-y)}$ with $0.85 \leqslant y \leqslant 1.00$ an extremely poor rate-capability is found whereas below 85 atom % Mg the rate-capability is excellent. A possible explanation can be found in the crystallography of these alloys, as has been reported in the past.[13,15,16] There, it was shown that hydrided Mg-based alloys with a Mg-content below 85 atom % have a fluorite-type structure, whereas for higher Mg-contents they crystallize in the rutile-type structure, commonly observed for MgH_2. Research is currently in progress to monitor the crystallography in situ as a function of H and Mg-content.

Finally, apart from a high gravimetric energy density, a good cycle-life performance is one of the main requirements for future applications. The electrochemical cycle-life behavior is measured by applying a high-rate and, subsequently, a low-rate discharge current of 0.12 mA (~1000 mA/g) and 0.012 mA (~100 mA/g), respec-

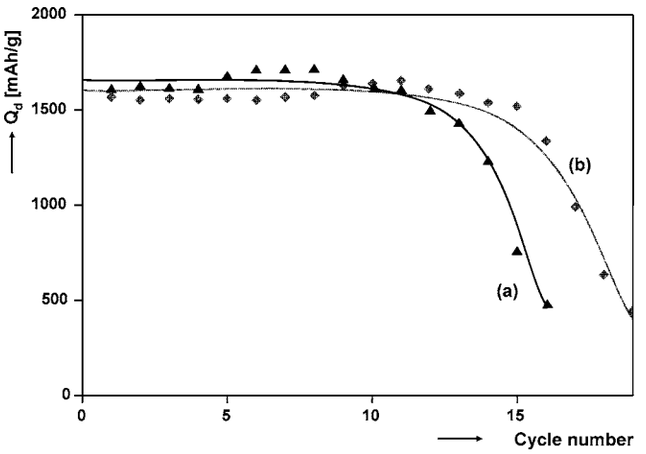

Figure 5. Discharge capacity (Q_d) determined by high-rate (+0.12 mA) and additionally low-rate (+0.012 mA) dehydrogenation vs cycle number for (a) electron beam deposited and (b) sputtered $Mg_{80}Ti_{20}$ thin films.

tively. The results of $Mg_{0.80}Ti_{0.20}$ alloys prepared by both deposition techniques are depicted in Fig. 5. Up to 11 cycles the EBD films reveal a nearly constant reversible hydrogen storage capacity which, hereafter, slowly decreases (curve a). However, the declining reversible H capacity is by no means related to the intrinsic storage capacity as the metallic films were delaminating after 11 cycles as reported before.[15] For the sputtered compounds (curve b), the reversible capacity is approximately constant up to 15 cycles. Beyond 15 cycles, delamination also causes the reversible hydrogen storage capacity to decrease. The somewhat better cycle-life of the sputtered films compared to that of the e-beam deposited alloys is related to their stronger adhesion to the substrate. Aside from this observation, gas phase (de)hydrogenation has shown that the cycle-life of sputtered Mg-Ti alloys easily surpasses 100 cycles, indeed revealing the perfect intrinsic recycle-ability properties of these MgTi hydrogen storage compounds.[24]

Conclusions

The influence of the preparation method (sputtering and EBD) on the metallurgy and electrochemical hydrogen storage properties of metastable $Mg_yTi_{(1-y)}$ has been studied in detail. Only minor differences in the crystallography of the as-deposited films have been found. Although the unit cell dimensions are identical, for sputtered films the grain size is found to be larger and the preferred orientation is somewhat stronger.

The hydrogen storage properties of EBD and co-sputtered alloys have been studied electrochemically. In spite of the fact that the overpotential is somewhat lower in the case of sputtered films, the overall response is found to be independent of the deposition technique. Moreover, a very similar compositional dependence on the rate-capability is found, indicating two specific regions that could be related to a fluorite-type structure for $Mg_yTi_{(1-y)}$ with $y < 0.85$ atom %. Above this critical composition, the diminishing rate-capability indicates the formation of the rutile-type MgH_2 structure. Finally, an analogous cycle-life behavior is found for the two methods. The diminishing discharge capacity of the compounds after about 12 cycles is related to the delamination of the metallic films from the substrate.

Acknowledgments

The authors thank T. Dao and Y. Tamminga for the RBS measurements. Furthermore, R. Bakker, P. Graat, and H. Wondergem are acknowledged for the XRD results. Financial support by the ACTS "Sustainable Hydrogen" program is gratefully acknowledged.

Eindhoven University of Technology assisted in meeting the publication costs of this article.

References

1. H. Senoh, K. Morimoto, H. Inoue, C. Iwakura, and P. H. L. Notten, *J. Electrochem. Soc.*, **124**, 2451 (2000).
2. P. H. L. Notten, in *Interstitial Intermetallic Alloys*, F. Grandjean, G. J. Long, and K. H. J. Buschow, Editors, p. 151, NASA (1995).
3. O. Arnaud, P. Barbic, P. Bernard, A. Bouvier, B. Knosp, B. Riegel, and M. Wohlfahrt-Mehrens, *J. Alloys Compd.*, **330–332**, 262 (2002).
4. H. Ye, B. Xia, W. Wu, K. Du, and H. Zhang, *J. Power Sources*, **111**, 145 (2002).
5. A. Singh, B. K. Singh, D. J. Davidson, and O. N. Srivastava, *Int. J. Hydrogen Energy*, **29**, 1151 (2004).
6. http://www.eere.energy.gov/hydrogenandfuelcells/mypp/
7. K. H. J. Buschow, P. C. P. Bouten, and A. R. Miedema, *Rep. Prog. Phys.*, **45**, 937 (1982).
8. R. W. P. Wagemans, J. H. van Lenthe, P. E. de Jongh, A. J. van Dillen, and K. P. de Jong, *J. Am. Chem. Soc.*, **127**, 16675 (2005).
9. H. Baker, Editor, *ASM Handbook—Alloy Phase Diagrams*, Vol. 3, ASM International, Materials Park, OH (1992).
10. D. Kyoi, T. Sato, E. Rönnebro, N. Kitamura, A. Ueda, M. Ito, S. Katsuyama, S. Hara, D. Noreus, and T. Sakai, *J. Alloys Compd.*, **372**, 213 (2004).
11. D. Kyoi, T. Sato, E. Rönnebro, Y. Tsuji, N. Kitamura, A. Ueda, M. Ito, S. Katsuyama, S. Hara, D. Noreus, and T. Sakai, *J. Alloys Compd.*, **375**, 253 (2004).
12. D. Kyoi, E. Rönnebro, N. Kitamura, A. Ueda, M. Ito, S. Katsuyama, and T. Sakai, *J. Alloys Compd.*, **361**, 252 (2003).
13. W. P. Kalisvaart, R. A. H. Niessen, and P. H. L. Notten, *J. Alloys Compd.*, In press.
14. R. A. H. Niessen and P. H. L. Notten, *Electrochem. Solid-State Lett.*, **8**, A534 (2005).
15. P. Vermeulen, R. A. H. Niessen, and P. H. L. Notten, *Electrochem. Commun.*, **8**, 27 (2006).
16. P. H. L. Notten, M. Ouwerkerk, H. van Hal, D. Beelen, W. Keur, J. Zhou, and H. Feil, *J. Power Sources*, **129**, 45 (2004).
17. D. M. Borsa, A. Baldi, M. Pasturel, H. Schreuders, P. Vermeulen, P. H. L. Notten, B. Dam, and R. Griessen, *Appl. Phys. Lett.*, In press.
18. R. A. H. Niessen and P. H. L. Notten, *Electrochim. Acta*, **50**, 2959 (2005).
19. R. A. H. Niessen and P. H. L. Notten, *J. Electrochem. Soc.*, **152**, A2051 (2005).
20. A. R. West, *Solid State Chemistry and Its Applications*, 1st ed., p. 367, John Wiley & Sons, New York (1984).
21. T. J. Richardson, B. Farangis, J. L. Slack, P. Nachimuthu, R. Perera, N. Tamura, and M. Rubin, *J. Alloys Compd.*, **356–357**, 204 (2003).
22. B. Farangis, P. Nachimuthu, T. J. Richardson, J. L. Slack, B. K. Meyer, R. C. C. Perera, and M. D. Rubin, *Solid State Ionics*, **165**, 309 (2003).
23. L. S. Birks and H. Friedman, *J. Appl. Phys.*, **17**, 687 (1946).
24. M. Slaman, B. Dam, M. Pasturel, D. M. Borsa, H. Schreuders, J. H. Rector, and R. Griessen, *Sens. Actuators B*, Submitted.